#### Wesleyan University

## Big Disk Energy

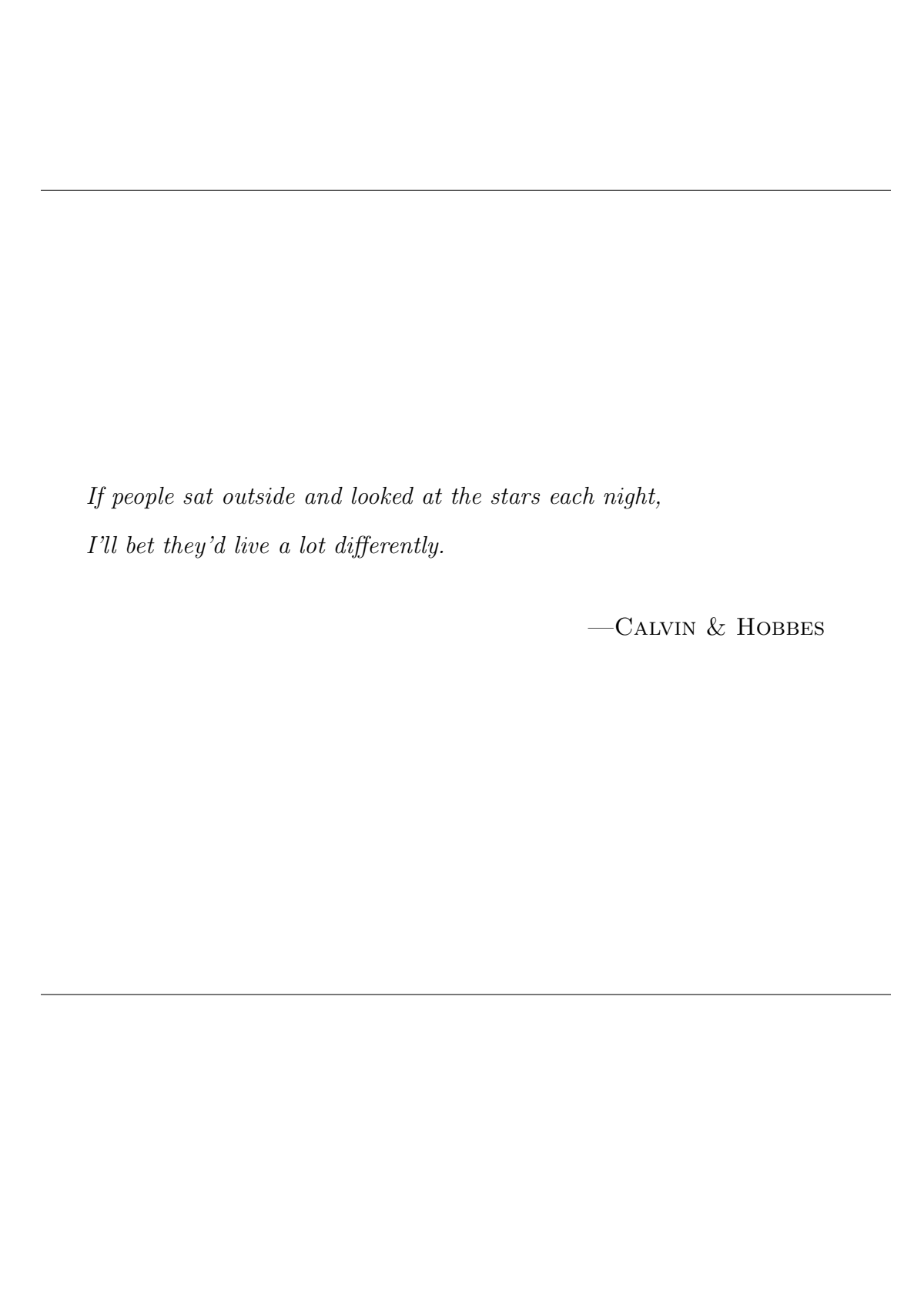
by

Jonas Powell Class of 2019

A thesis submitted to the faculty of Wesleyan University in partial fulfillment of the requirements for the Degree of Master of Arts

Middletown, Connecticut

April, 2018



# Acknowlegdements

Thanks!

## Contents

A	ckno	wlegdements	ii		
1	Intr	oduction	1		
2	Obs	ervations	2		
3	Results				
	3.1	Modeling	4		
4	Res	ults	10		
	4.1	Reduction Strategies	10		
5	Results 11				
	5.1	Reduction Strategies	11		
6	Con	aclusion	12		
	6.1	Something	12		
	6.2	Future Work	12		
	6.3	Prospects of the field	12		
	6.4	Acknowledgments	12		
Bi	bliog	graphy	13		

# Chapter 1 Introduction

#### Observations

The data presented in this thesis are part of an ALMA survey of Orion proplyds in Orion (project 2011.0.00028.S); data collection and analysis methods of the continuum results are presented in Mann et al. (2014). Since this was part of a Cycle 0 Early Science project, the survey used only 22 of the array's 12 meter dishes in a hybrid configuration, with baselines ranging from 21.2 to 384.2 meters, yielding maximum angular scales and angular resolution of 8" and 0."5, respectively. At a distance of 389 pc, max angular scales and angular resolution correspond to 3,112 AU and 194 AU, respectively. The distance to the stars used here was recently measured by Gaia (Collaboration (2016), Collaboration et al. (2018)) to be  $389 \pm 7.97$ , nearer than the previous measurement of 414 pc.

Observations were made in Band 7 in four 1.875 GHz-wide bands arranged to cover the rest frequencies of the HCO+ (4-3), HCN (4-3), CO (3-2), and CS (7-6) transitions (356.734 GHz, 354.505 GHz, 345.796 GHz, and 342.883 GHz, respectively). Each band was split into 3840 channels with width 488.28 kHz, yielding a velocity resolution of 0.42 km s<sup>-1</sup>.

Analysis showed that excluding baselines shorter than 110 k $\lambda$ , 80 k $\lambda$ , and 60 k $\lambda$  for HCO<sup>+</sup>, HCN, and CO respectively optimized signal-to-noise ratios for each data set. The CS line showed no improvement with baseline cutting. This process is explained in greater detail in the Results chapter. more here? i.e. resolution

2. Observations 3

or something

These data, from Field 4 of Mann et al. (2014) represent 13.6 minutes of onsource time. This duration was split into six 136 second observations, spaced out over 7.5 hours to ensure adequate uv coverage. With the esulting in a synthesized beam of 0."57×0."51 with a position angle of 85°. Precipitable water vapor in the atmosphere was stable at 0.7 mm.

The data were calibrated by ALMA staff using standard procedures in the Common Astronomy Software Applications (CASA, citation). The antenna-based complex gains and bandpass response of the system were calibrated using observations of the quasars J0607-085 and J0522-364 respectively. The absolute flux calibration was determined from observations of Callisto. The model of Callisto was drawn from Butler (2012) (citation). Absolute flux calibration is estimated to be accurate to within 10% (Mann et al. (2014)).

The velocity reference frame was converted from CASA's standard topocentric frame to LSRK (kinematic local standard of rest) using the CASA task cvel. Next, continuum emission was subtracted in the uv plane using the CASA task contsub. Visibilities were then inverted with natural weighting, deconvolved, and restored using standard procedures from the Multichannel Image Reconstruction Image Analysis and Display, or MIRIAD, package (RJ Sault (1995))

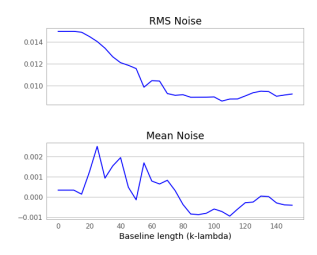
#### Results

#### 3.1 Modeling

Spatially and spectrally resolved line emission was detected for CO (3-2), HCO<sup>+</sup> (4-3), HCN (4-3), and CS (7-6) across around 50 channels of width 0.42 km s<sup>-1</sup>. Before beginning modeling processes, it is useful to the data as the are. This process includes removing cloud contamination, investigating the general morphology of the disks using moment maps, estimating the disks' gas masses using integrated line flux, and examining the velocity profile to estimate the mass of the central star (really?).

Cloud contamination occurs when emission from background or foreground gas clouds is detected in the same direction as the disk being observed. Since the Orion Nebula has a higher gas density than low-mass SFRs, cloud contamination is more much common and problematic. "Previous observations of these disks by Mann Williams (2009) (citation) (do I have these?) strongly detected the CO (3-2 line)". Thanks to the higher sensitivity of the ALMA observations, etc.

HCO<sup>+</sup> displayed the most significant cloud contamination, thanks to its low critical density and higher abundance in the clouds. For the other molecular lines, which have higher critical densities, cloud contamination is less severe but still clearly present in HCO<sup>+</sup>, which is the brightest tracer.



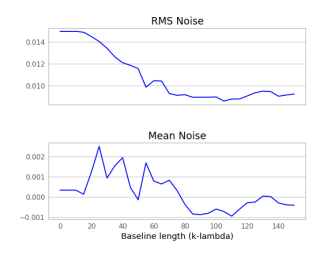


**Figure 3.1:** First moment map of HCO+,**Figure 3.2:** First moment map of HCN, with and without (below and above, respectively) baseline cuts.

Since cloud contamination inherently tends to be large-scale in structure, excluding short baselines reduces its contribution to the observations. While this process slightly reduces the total recovered flux from the disk and our ability to characterize its large-scale structure, it is necessary to avoid including cloud emission from the cloud in the process of fitting the disk emission. By evaluating mean and RMS noise for an off-source region of the field while varying the minimum baseline used, we found that excluding baselines less than 110 k $\lambda$ , 80 k $\lambda$ , and 60 k $\lambda$  for HCO<sup>+</sup>, HCN, and CO, respectively, yielded optimum results. Since the CS line already has a very low SNR and a higher critical density, excluding baselines did not improve the observations.

Line	Baselines (")	Max Angular Scale (")	Integrated Line Flux (Jy km $s^{-1}$ )
CS (7-6)	All	8."5	0."47
CO (3-2)	All	8."4	0."47
CO (3-2)	$>$ 60 k $\lambda$	3."4	0."47
HCN (4-3)	All	8."2	0."45
HCN (4-3)	$>$ 80 k $\lambda$	2."6	0."45
$HCO^{+}$ (4-3)	All	8."2	0."45
$HCO^{+}$ (4-3)	$>$ 110 k $\lambda$	1."9	0."45

 ${\tt Noise-copmarison-HCO+\_mom0.pdf}$ 

6

3. Results

Figure 3.3: blah

The effects of these exclusions are detailed in Table 1 and demonstrated on the HCO<sup>+</sup> line in Figure 1. (Analysis of these plots, bottom of p.3 in Factor et al)

In all lines, rotation of each disk is clearly visible as a transition from redshifted emission in one corner to blue-shifted emission in the other corner\*\*\*. The maximum extent of the 3- $\sigma$  contours along the disks' major axes correspond to outer diameters of the HCO+ disks of A and B; outer diameters of the HCN disks of A and B; and outer diameters of the CO disks of A and B, all at a distance of 389pc. The CS emission is not detected strongly enough to provide a reliable measurement (check that this is true)

Tables 2 and 3 present the velocity-integrated line fluxes and the best-fit parameters for a simple elliptical Gaussian fit to the visibilities for each disk, respectively. Integrated line flux was measured using the MIRIAD task egcurs to integrate the intensity in the zeroth-moment map throughout the region enclosed by the 3  $\sigma$  contour level. Uncertainties in the integrated line flux do not include the 10% absolute flux calibration uncertainty inherent in the ALMA observations caused by uncertainties inthe models of solar system objects used as flux callibrators. Elliptical Gaussian fits of the visibilities were performed using the MIRIAD task uvfit.

Assuming optically thin emission (maybe good?) and Local Thermodynamic Equilibrium (LTE), the line-emitting gas mass,  $M_{gas}$  is given by:

$$M_{\rm gas} = \frac{4\pi}{h\nu_0} \frac{Fmd^2}{A_{nl}X_n},\tag{3.1}$$

where F is the integrated line flux, m is the mass of the emitting gas molecule,

d is the distance to the source, h is the Planck constant,  $\nu_0$  is the molecular line's rest frequency,  $A_{ul}$  is the Einstein coefficient for the (u-l) transition, and

$$X_u = \frac{N_u}{N_{\text{tot}}} = (2J_u + 1) \frac{\exp[-B_0 J_u (J_u + 1) hc/kT_{\text{ex}}]}{kT_{\text{ex}}/hcB_0}.$$
 (3.2)

In (2),  $\frac{N_u}{N_{\text{tot}}}$  is the ratio of the number of molecules in the upper state to the total number of molecules;  $J_u$  is the quantum number of the upper level;  $B_0$  is the rotation constant in units of wavenumber; h and c are the Planck constant and speed of light, respectively; and  $T_{\text{ex}}$  is the excitation temperature. VALUES FOR  $A_U LANDBOWERETAKENFROMMOLECULARDATAMADEAVAILABLEBYSHOIER$ 

# A position-velocity diagram for HCO<sup>+</sup> is shown in Figure 4, showing the posi-

tion, as a function of velocity, of emission form a cut along the major axis of the

disk (FIGURE OUT HOW TO DO THIS). ANALYSIS of this stuff.

To find best fit values, we use disk modeling and ray-tracing code developed by ?. The code turns a set of paramters describing the disk's physical structure (atmospheric temperature, density structure, molecular abundances, and so on) into a three dimensional model. Given observational characteristics (distance, inclination, and so on), it can then turn that model into a simulated sky-projected image which may then be compared to our observational data.

Explorations of paramter space were implemented through

Things to get: \* Rewrite this whole thing. \* Previous observation of these disks with SMA? Maybe Mann Williams 2009. What did they detect? \* Integrated Flux Measurements \* Make a 2-image subplot of HCO+ with and without baseline cutting. Moment 0 or Moment 1? Show n-sigma contours \* Find max width of disks for each line by 3-sigma contour

\* Make moment0 and moment1 plotters. Two panel or just 1? Should have contouring. \* Use cgcurs to get integrated line flux in moment0 map. \* use uvfit for elliptical guassian vis fits. \* PV Diagram \* Gas mass calculations

# Results

4.1 Reduction Strategies

# Results

5.1 Reduction Strategies

## Conclusion

- 6.1 Something
- 6.2 Future Work
- 6.3 Prospects of the field

#### 6.4 Acknowledgments

This work has made use of data from the European Space Agency (ESA) mission Gaia (https://www.cosmos.esa.int/gaia), processed by the Gaia Data Processing and Analysis Consortium (DPAC, https://www.cosmos.esa.int/web/gaia/dpac/consortium). Funding for the DPAC has been provided by national institutions, in particular the institutions participating in the Gaia Multilateral Agreement.

## **Bibliography**

- Collaboration, G. 2016, Astronomy & Astrophysics, 595, A1, arXiv: 1609.04153
- Collaboration, G., Brown, A. G. A., Vallenari, A., Prusti, T., de Bruijne, J. H. J., Babusiaux, C., & Bailer-Jones, C. A. L. 2018, Astronomy & Astrophysics, 616, A1, arXiv: 1804.09365
- Factor, S. M., et al. 2017, The Astronomical Journal, 153, 233, arXiv: 1704.01970
- Goodman, J., & Weare, J. 2010, Communications in Applied Mathematics and Computational Science, 5, 65
- Mann, R. K., et al. 2014, The Astrophysical Journal, 784, 82, arXiv: 1403.2026
- Mann, R. K., & Williams, J. P. 2009, The Astrophysical Journal, 699, L55
- Ricci, L., Robberto, M., & Soderblom, D. R. 2008, The Astronomical Journal, 136, 2136
- Ricci, L., Testi, L., Williams, J. P., Mann, R. K., & Birnstiel, T. 2011, The Astrophysical Journal, 739, L8
- RJ Sault, MCH Wright, R. S. H. P. J. H. P. T. 1995, ASP Conf. Ser., 77, 433
- Sault, R. J., Teuben, P. J., & Wright, M. C. H. 2006, arXiv:astro-ph/0612759, arXiv: astro-ph/0612759
- Smith, N., Bally, J., Licht, D., & Walawender, J. 2005, The Astronomical Journal, 129, 382
- Williams, J. P., et al. 2014, The Astrophysical Journal, 796, 120, arXiv: 1410.3570